# Measurement and Modelling of Rotational Core Loss of Fe-Based Amorphous Magnetic Material under 2-D Magnetic Excitation

Pejush Chandra Sarker[1], Youguang Guo[1], *Senior Member, IEEE,* Hai Yan Lu[1], *Senior member, IEEE,* and Jian Guo Zhu[2], *Senior Member, IEEE*

[1]Faculty of Engineering and Information Technology, University of Technology Sydney, Australia
[2]School of Electrical and Information Engineering, The University of Sydney, Australia

**Fe-based amorphous magnetic materials are recently attracting strong interests for constructing high-power density and high-efficiency rotating electrical machines due to their attractive properties, such as low core loss and high magnetic saturation. Accurate measurement and modelling of the rotational core losses of the core magnetic materials, and the corresponding patterns of rotating magnetic flux density (B) and magnetic field strength (H) are important for the analysis and design of electrical machines. This paper presents the measurement of rotational core loss of a Fe-based amorphous magnetic material (Amorphous 1k101), and its corresponding modellings under two-dimensional (2-D) circularly and elliptically rotating magnetic fields. In addition, an improved and simplified analogical model of rotational hysteresis loss is proposed for such magnetic materials. The circular and elliptical B loci and the corresponding H loci have been investigated to acquire the perception of anisotropy and permeability of the amorphous materials. The proposed theory and models are experimentally verified.**

***Index Terms*—Amorphous magnetic material, 2-D magnetic properties, rotational core loss, magnetic hysteresis.**

## I. Introduction

The magnetic field in transformers generally varies with time which is known as alternating magnetic field that can also be defined as one-dimensional (1-D) magnetic field since the magnetic field is considered as only time varying along a fixed orientation. On the other hand, for some cases, e.g. the rotating electrical machines and the T-joint of the three-phase transformers, the magnetic field varies with respect to both time and orientation [1], [2], and the dissipated power in the magnetic core due to the rotating magnetic field is different from that caused by the alternating magnetic field. In many rotating electrical machines, the rotational stator core loss can be accounted for up to half of the total core losses [2]. Therefore, it is important to take into account the rotational core losses of magnetic materials so that the proper thermal and laminated insulation specifications can be contemplated in the design of the electrical machines.

Recently, various rotating electrical machines of amorphous material cores were reported by different researchers [3]-[5] due to their low core loss property especially compared to the silicon steel sheets. Among the Fe-based, Co-based and Ni-based amorphous magnetic materials, the Fe-based amorphous material is most commonly utilized in electrical machines due to its higher saturation magnetic flux density ($B_s$) and lower price. There are many Fe-based amorphous magnetic suppliers over the world, e.g. Hitachi Metals Ltd., Japan, and Henan ZY Amorphous Technology Co. Ltd., China. In this research, the Zhongyue amorphous 1k101 metal [6], [7], produced by Henan ZY Amorphous Technology Co. Ltd., is used for the investigation of two-dimensional (2-D) rotational core loss. The selected amorphous material consists of 80% Fe, and 20% SiC and B metal elements [6]. Strip-casting technology is exploited to manufacture the amorphous strip [6]. The strip-casting technology is a type of near-net-shape casting processes where molten alloy composition is solidified when it touches cold rotating surfaces [8]. The fast cooling process is used for the amorphous state of the alloy [9]. However, in order to improve the magnetic properties, the annealing process such as transverse field annealing, longitudinal field annealing or no field annealing, is generally carried out on the material. No field annealing process is considered for the material in this study.

In 1896, the first measurement technique of the rotational core loss was developed by Baily [10], where the developed torque, which is imposed on the magnetic material specimen by the rotational magnetic field, is firstly measured, and the corresponding loss is then calculated from the measured torque. In the last hundred years, different 2-D core loss testing devices such as the square specimen tester (SST), disk specimen tester and large sheet-based tester were developed by different researchers [2], [11]-[13].

The 2-D core losses of soft magnetic composite materials and silicon steels were investigated and modelled by different researchers [14]-[16]. The 2-D vector magnetic properties of Metglas 2605 HB1 and Metglas 2650S-2 amorphous materials were examined at constant frequencies in [17] and [18] respectively. However, core loss modellings were not carried out in these works. For modelling of rotational hysteresis core loss, two empirical methods are commonly utilized: one is founded on the analogical approach [19] and the other on alternating measured core loss data [20]. The analogical model

of rotational hysteresis loss shows better accuracy than the model obtained from the alternating loss data. In addition, the analogical rotational hysteresis model is independent of the alternating measured hysteresis loss. However, the first method basically uses the torque equation of a single-phase induction motor to model the rotational hysteresis loss, as its torque-slip relation is similar to the relation between rotational hysteresis loss and magnetic flux density. In the same way, it is observed that the equation of developed mechanical power of a three-phase induction motor, which also shows similar patterns to the rotational hysteresis loss, is more simplified than the torque equation of the single-phase induction motor. Therefore, it is a great aspect to use the developed mechanical power equation of a three-phase induction motor to model the rotational hysteresis loss for not only simplifying the approach but also improving the accuracy. Since the eddy current and excess losses occur simultaneously with hysteresis loss for an alternating excitation, their modellings are also included with hysteresis loss models to obtain the total loss under both circular and elliptical rotating magnetic fields. However, the modelling of 2-D magnetic rotational core loss of any amorphous metal has not been found in the literature.

In this paper, the 2-D vector magnetic properties of a Fe-based amorphous magnetic material (Amorphous 1k101) has been investigated under 2-D rotating magnetic fields. The key contributions of this paper are: (i) measurement of the rotational core losses of the selected magnetic material at different magnetic flux densities and frequencies; (ii) investigation of other magnetic properties, e.g. the loci of magnetic flux density (**B)** and magnetic field strength (**H)** vectors under the rotational magnetic fields; (iii) proposal of an improved and simplified analogical model of the rotational hysteresis loss; (iv) modelling of the total rotational core loss of the magnetic material by incorporating the rotational eddy and excess loss models with the proposed hysteresis model; and (v) investigation of effects of the changes of major and minor axes of the **B** loci on the total loss of the material. The proposed model is verified by considerable agreement between experimental and simulation results. The measurement data and proposed model can be very useful for designing the rotating electrical machines.

## II. Rotational (2-D) Core Loss Testing System

### *A. Square Specimen Tester*

The square specimen tester (SST) initiated by Brix [11] is favorable for measuring 2-D core loss due to the flexible control system, more uniform magnetic field and higher accuracy than any other conventional measurement systems. A single sheet SST [2], [21] is utilized here to explore the 2-D vector magnetic properties of the selected amorphous material. The corresponding block diagram of the 2-D experimental set-up is shown in Fig. 1. The SST consists of yokes made of vertically laminated grain-oriented silicon steel sheets. The shapes of the yokes were constructed in such a way that the tester has four wedge type magnetic poles**.** Two sets of excitation coils are arranged on X and Y-axes magnetic poles, and each set has two coils, which are connected in series. Each coil consists of 300 turns of 1.6 mm insulated copper wire. In the middle of the tester, a square specimen of the material is placed as shown in Fig. 1. The rotating magnetic field is then generated around the specimen by exciting both groups of exciting coils. Labview is used for data acquisition and generating the two channel excitation signals of 90º phase difference to produce rotational magnetic fields. The rotating magnetic field generated by the tester induces the magnetization in the specimen, and the induced magnetizations are then measured by **B** and **H**-sensing coils for both axes, respectively.

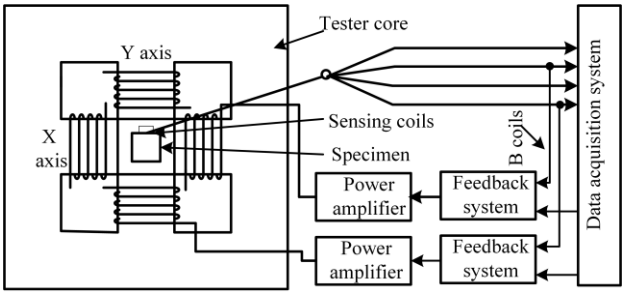


Fig. 1. Block diagram of 2-D square specimen testing system [21].

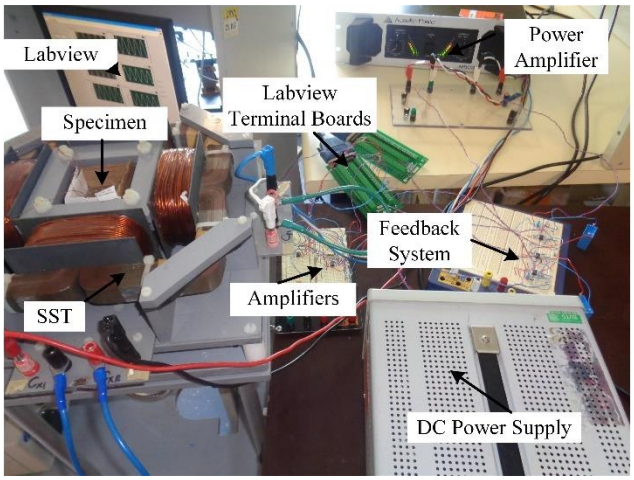


Fig. 2. A photo of the 2-D core loss measurement set-up.

A feedback system is employed to control the shape of the induced voltage in the **B**-sensing coils. A two-channel power amplifier is used in the testing system to amplify the voltage as well as power of the output signals of the feedback system so that they can excite the coils of the tester. A photo of the 2-D rotational core loss measurement system is shown in Fig. 2. The specimen was cut from the AMCC-320 [7] amorphous core which is made of amorphous 1k101 strips, and the dimensions of the specimen are 50 mm × 50 mm × 0.86 mm. As the thickness of an amorphous strip of the core is about 25 μm which indicates that the specimen, whose thickness is 0.86 mm, consists of a stack of amorphous strips. The stacking factor of the specimen is the same as that of the core which is about 85%.

### B. *Measurement Methods for* **B** *and* **H**

The core loss is measured using the field-metric method where the measurements of **B** and **H** are firstly required to be measured, and the loss is then calculated from them. **B** and **H** are measured from sensing coils which are placed around the specimen. However, the voltages induced in **H**-sensing coils are normally very small especially at low frequency and low magnetic flux density. Therefore, precision operational amplifiers for both types of sensing coils are utilized to overcome the low voltage measurement problems.

The **B**-sensing coils are wound over the middle of the specimen so that one coil is positioned in the X-axis direction and the other in the Y-axis direction. Each coil consists of 15 turns of 0.1 mm enamel insulated copper wire. The components of **B** on each axis are then calculated by the following equation [2], respectively:

$$B_i = \frac{1}{K_{Bi}} \int v_{Bi} dt \qquad i = x, y \tag{1}$$

where $K_{Bi}=K_s N_{Bi} F_{Bi} d_{th} d_{lw}$ are the coefficients of $B_i$-sensing coils, $N_{Bi}$ the number of turns of the sensing coils, $F_{Bi}$ the amplification factors, $K_s$ the stacking factor, $d_{th}$ the thickness of the specimen, $d_{lw}$ the length or width of the specimen, and $v_{Bi}$ the induced voltages on sensing coils.

The **H**-sensing coil on each axis consists of 153 turns of 0.06 mm enamel insulated copper wire which are wound over a 0.50 mm plastic former. The components of **H** on each axis are then calculated by the following equation [2], respectively:

$$H_i = \frac{1}{\mu_0 K_{Hi}} \int v_{Hi} dt \qquad i = \mathrm{x}, \mathrm{y} \tag{2}$$

where $\mu_0$ is the permeability of air, $v_{Hi}$ the induced voltages in the sensing coils, and $K_{Hi}$ the $H_i$-sensing coil coefficients which are determined by calibration of the sensing coils [2].

### C. *Feedback System*

The magnetization on ferromagnetic materials shows a non-linear relationship with the magnetic field strength especially at the vicinity of the magnetic saturation point. Consequently, the magnetic flux density becomes non-sinusoidal in spite of sinusoidal excitation voltage. Therefore, the rotating magnetic flux density **B** no longer exists as circular. To obtain a circular rotating **B**, a feedback differential circuit on each axis is added in the testing system. A differential amplifier is mainly exploited as the feedback system which receives the differential input obtained from Labview and amplified **B**-sensing coil signals as shown in Fig. 3. In addition, a high pass filter and a low pass filter are used to decrease the drift voltage, and eliminate the high-frequency interferences, respectively. Finally, the gain of the power amplifier is adjusted in such a way so that the output of **B**-sensing coil becomes sinusoidal.

## III. Core Loss Measurement under Different Excitation Conditions

### A. *Circularly Rotating Core Loss Measurement*

If a rotating magnetic field is imposed on a magnetic material specimen, power dissipation happens, which can be theoretically derived from Poynting's theorem [2]. Accordingly, the loss dissipated in the specimen is obtained by the following equation,

$$P_t = \frac{1}{T\rho} \int_0^T \left( H_x \frac{dB_x}{dt} + H_y \frac{dB_y}{dt} \right) dt \tag{3}$$

where $P_t$ is the total core loss (W/kg), $T$ the time period (s), $\rho$ the mass density (kg/m$^3$), $H_x$ and $H_y$ the components of **H**, and $B_x$ and $B_y$ the components of **B,** respectively. Fig. 4 shows the rotational core losses of the magnetic material at different frequencies and different maximum magnetic flux densities ($B_m$). It is noticed from Fig. 4 that the loss increases with the increase of the **B** except when it is near to the magnetic saturation region especially at low frequencies, e.g. 5 Hz, 10 Hz and 20 Hz. In those cases, the core loss decreases slowly due to the annihilation and formation of the magnetic domain walls.

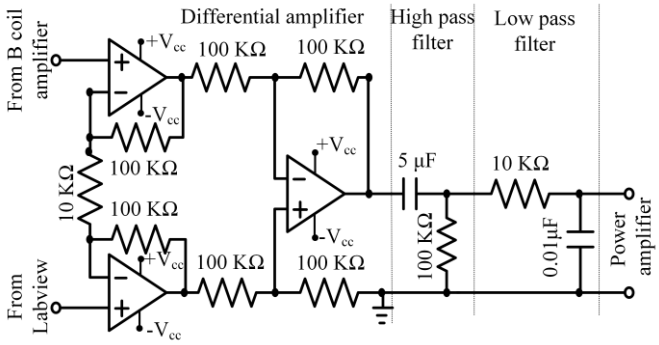


Fig. 3. Feedback system on each axis used for the 2-D magnetic property measurement system [2].

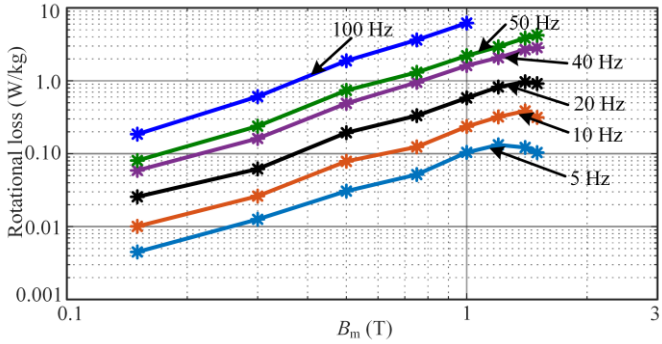


Fig. 4. Rotational core losses of the amorphous magnetic material with $B_m$ for different frequencies.

Fig. 5 shows the controlled circular loci of **B** and the corresponding loci of **H** at different magnetic flux densities under 50 Hz rotating magnetic fields. It is noticed from Fig. 5(b) that the loci of **H** are not circular as the permeability of the amorphous material varies with both **H** and **B**. In addition,

the maximum values of $H_x$ and $H_y$ are not exactly the same, which indicates that the permeability of the magnetic material in X and Y-directions differs slightly.

### *B. Alternating Core Loss Measurement*

The above mentioned 2-D core loss testing system can also be utilized to measure the alternating loss of the magnetic material. In this case, the excitation coils on X and Y-axes of the tester are excited separately, and their corresponding core losses are measured. The alternating losses on X-axis (Transverse direction) and Y-axis (Rolling direction) differ slightly from each other due to the anisotropy of the magnetic material. Therefore, the average value of them can be used as the final alternating core loss of the material. Fig. 6 shows the B-H loops in both directions with the peak value of 1.40 T under 50 Hz sinusoidal voltage excitation. It is observed from Fig. 6 that the B-H loops for X and Y-axes directions are slightly different. Therefore, the corresponding permeabilities are not the same which indicates that the selected magnetic material shows anisotropy property. However, the alternating loss always shows an increasing trend with the increase of $B_m$ at any operating frequency as shown in Fig. 7.

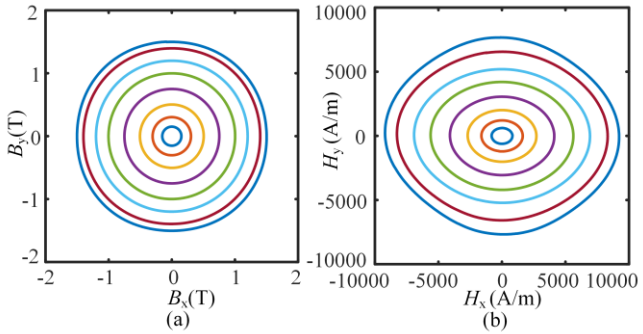


Fig. 5. (a) Loci of **B** and (b) the corresponding loci of **H** at different magnetic flux densities under 50 Hz excitation.

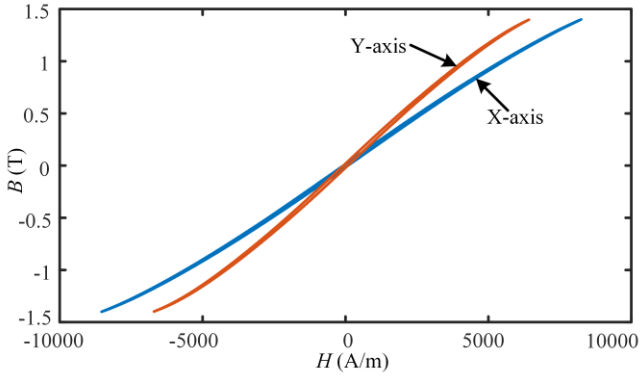


Fig. 6. B-H loops under alternating magnetic field at 50 Hz and peak value of magnetic flux density 1.40 T on X and Y-axes.

Figs. 8 and 9 show the alternating and rotational core losses of the amorphous material at 50 Hz for different magnetic flux densities respectively. From the figures, it is observed that the rotational core loss ($P_r$) is always higher than the alternating core loss ($P_{alt}$) for the same value of $B_m$. It is observed from the measured core loss data that the ratio of the rotational and alternating core losses ($P_r/P_{alt}$) of the magnetic material at 50 Hz remains nearly 1.90 with some fluctuations for $B_m$ up to 1 T, and after that it decreases dramatically. There are mainly two reasons for the significant reduction of the ratio: (i) the rotational hysteresis loss decreases dramatically at the vicinity to the saturation region, and (ii) the sharp increase of the alternating loss in the magnetic saturation region. In addition, the rotating excess loss coefficient changes slightly with the change of $B_m$ (details in Section IV.C), which also affects the ratio.

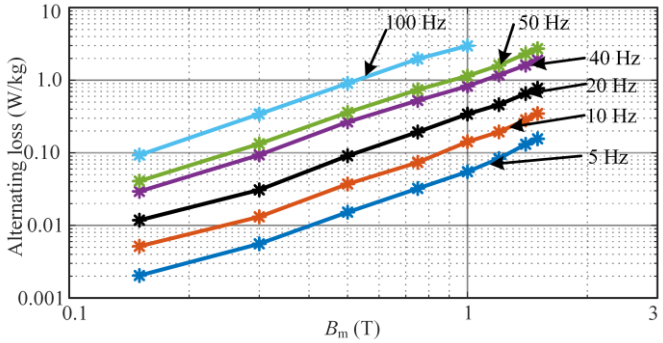


Fig. 7. Alternating core losses of the amorphous magnetic material with $B_m$ for different frequencies.

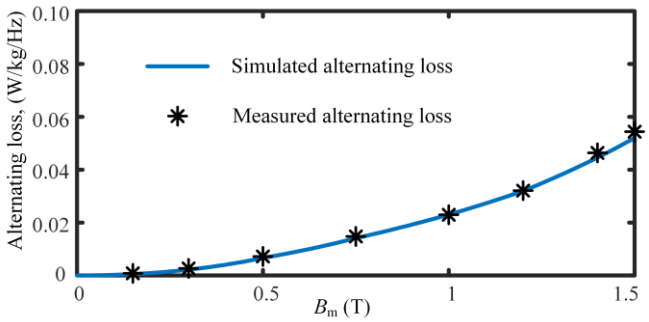


Fig. 8. The alternating core losses of the amorphous material with $B_m$ under 50 Hz sinusoidal excitation.

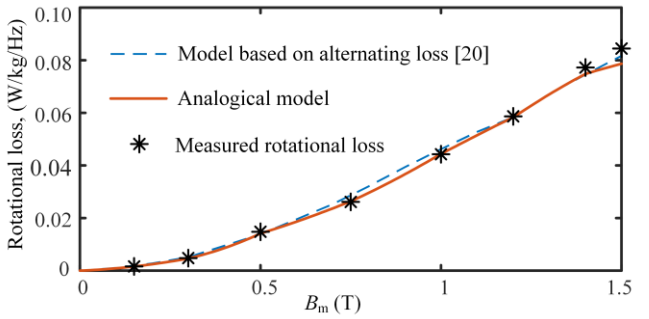


Fig. 9. The rotational core loss of the amorphous material with $B_m$ under 50 Hz rotating magnetic field.

### *C. Elliptical Core Loss*

For elliptically rotating magnetic field, the values of $B_m$ at the major and minor axes of elliptical loci of **B** differ from each other. Consequently, both the rotational and alternating core losses exist in the total loss. Their shares in the total loss depend on the axis ratio of the loci of **B**. However, the elliptical loss is measured by keeping the major axes on one axis and the minor axes on another axis as shown in Fig. 10.

Fig. 11 shows the average elliptical loss with the axis ratio of the loci of **B**. In Fig. 11, $B_m$ for the major axis is considered as 1.20 T, and $B_m$ for the minor axis varies discretely from 0 to 1.2 T. From Fig. 11, it is observed that when only one of the axes is excited, the loss becomes equal to the alternating core loss. After that the loss increases with the increase of the axis ratio although the increasing trend is not linear. At the low value of the axis ratio, the loss changes slowly with the change of axis ratio but at a high value of the axis ratio the loss changes rapidly with the change of the axis ratio. When the minor and major axes of loci **B** are equal, the elliptical loss becomes equal to the circular rotational loss.

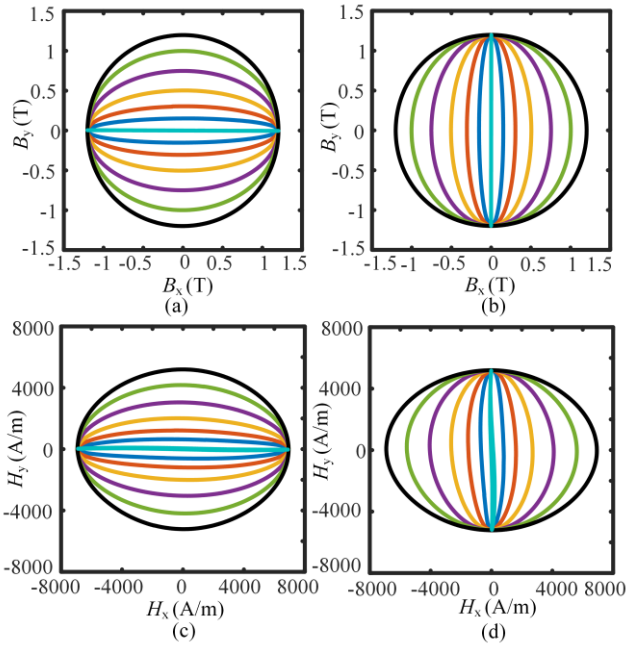


Fig. 10. Elliptical loci of **B** at 50 Hz when major axis is on (a) X-axis and (b) Y-axis, and the corresponding loci of **H** when major axis is on (c) X-axis and (d) Y-axis.

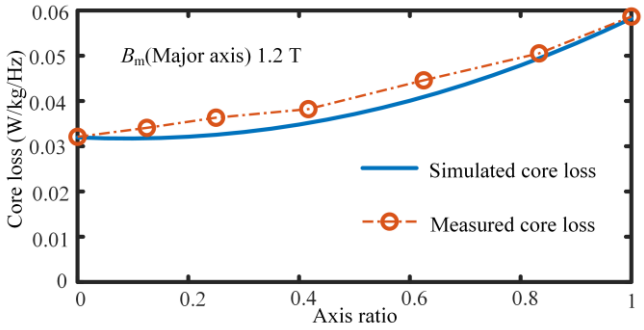


Fig. 11. Total core loss with different axis ratios at 50 Hz excitation.

## IV. Modelling of Rotational Core Loss

Loss separation method is exploited to model the core loss. In the loss separation method, hysteresis, eddy current and excess losses are modelled separately, and after that they are combined to obtain the total rotational core loss which are discussed below.

### A. Rotational Hysteresis Loss Model

*1) Existing Rotational Hysteresis Loss Models*:

An analogical rotational hysteresis model was proposed in [19], which is based on the equation of torque-slip relation of a single-phase induction motor. By using the analogical approach, the rotational hysteresis loss per frequency ($P_{hr}/f$) can be modelled as follows [19]:

$$P_{hr}/f = a_1\left[\frac{1/s}{(a_2+1/s)^2+a_3}-\frac{1/(2-s)}{\{a_2+1/(2-s)\}^2+a_3}\right] \quad (4)$$

with

$$s = 1-\frac{M}{M_s}\sqrt{1-\frac{1}{a_2^2+a_3}} \quad (5)$$

where $M$ is the amplitude of magnetization vector **M** (**M**=**B**/$\mu_0$-**H**), $M_s$ is the saturation magnetization, and $a_1$, $a_2$ and $a_3$ are constants. Since it can be generally considered as $M >> H$, $M/M_s$ in (5) can be replaced by $B_m/B_s$ [14].

Another method was postulated in [22], where the rotational core loss could be supposed to the sum of alternating losses in both axes under the same magnetic flux density. Unfortunately, this approach cannot be directly used for rotational hysteresis loss as the rotational hysteresis loss near to the saturation magnetic flux density shows different characteristic compared to that of alternating loss. To solve the problem, the method was modified in [20] where an approximate modification factor is included in the calculation as follows

$$P_{hr} = (1-a_m)\{P_{alt}(B_{lm})+P_{alt}(B_{sm})\} \quad (6)$$

where $P_{alt}$ is the alternating loss in W/kg, and $a_m$ is the modification factor calculated using measured data, $B_{lm}$ and $B_{sm}$ are the maximum magnetic flux densities in major and minor axes, respectively.

*2) Proposed Rotational Hysteresis Loss Model*: The proposed model is an analogical approach which is based on equation of mechanical power developed on a three-phase induction motor. The developed power ($P_m$) in the motor can be calculated by the following equation [23]:

$$P_m = \frac{3\omega_r V_{th}^2 R_2/s}{\omega_s\left[(R_{th}+R_2/s)^2+(X_{th}+X_2)^2\right]} \quad (7)$$

where $\omega_r = (1\text{-}s)\omega_s$, and $V_{th}$, $X_{th}$, $R_{th}$, and $\omega_s$ are the parameters related to the motor. By using the analogical approach, the rotational hysteresis loss per frequency can be obtained by

$$P_{hr}/f = \frac{b_1(1\text{-}s)s}{\left[(b_2 s+1)^2+b_3 s^2\right]} \quad (8)$$

with

$$s = 1 - \frac{B_m}{B_s} \tag{9}$$

From (8) and (9), it is observed that the proposed analogical rotational hysteresis loss model is more simplified than the existing analogical rotational hysteresis model [19] as shown in (4) and (5).

### B. Modelling of Rotational Eddy Current Loss

Eddy current loss appears due to the micro-eddy currents generated near to the moving domain walls. Since the thickness of the amorphous sheet is much smaller than that of silicon steel, the eddy current loss of the amorphous material slightly affects the total loss as shown in Fig. 12. Thus, the skin effect on the material in the low and medium frequency ranges can be neglected. For modelling of the rotational eddy current loss, the classical model can be used which is as follows [22]:

$$P_{er} = 2\frac{\sigma\pi^2 d^2}{6\rho} B_m^2 f^2 \tag{10}$$

where $P_{er}$ is the rotational eddy current loss in W/kg, $\sigma$ the conductivity of the amorphous sheet, $d$ the thickness of amorphous sheet, $f$ the frequency, $\rho$ the mass density and $B_m$ the maximum magnetic flux density. The conductivity is defined as reciprocal of resistivity. The resistivity of the amorphous material studied in this paper is 130 μΩ.cm [7]. The value of mass density of the material is 7180 kg/m$^3$.

### C. Modelling of Rotational Excess Loss

Rotational excess loss can be modelled by two ways: one is the conventional analytical model [19], and the other is obtained from measured alternating excess loss data [20]. In this study, the first one, i.e. conventional excess loss model is incorporated with the analogical rotational hysteresis model. The conventional rotational excess or anomalous loss $P_{ar}$ (W/kg) can be obtained by

$$P_{ar} = C_{ar} B_m^{1.5} f^{1.5} \tag{11}$$

where $C_{ar}$ is the rotational excess loss coefficient. Therefore, the total rotational core loss can be obtained as follows:

$$P_r = P_{hr} + 2\frac{\sigma\pi^2 d^2}{6\rho} B_m^2 f^2 + C_{ar} B_m^{1.5} f^{1.5} \tag{12}$$

where both $P_{hr}$ and $C_{ar}$ are unknown which can be obtained by extrapolation and curve fitting of the measured core losses. Fig. 12 shows the curve fitting of the measured core losses per frequency ($P_r/f$) with $f$ for different $B_m$, where $P_r$ is obtained from (12). The separation of the rotational hysteresis loss from the total loss at different magnetic flux densities is also observed in Fig. 12. Thus, $C_{ar}$ and $P_{hr}$ for the whole magnetic flux density range can be obtained as shown in Figs. 13 and 14 respectively. From Fig. 13, it is observed that rotating excess loss coefficient changes with the magnetic flux density. Consequently, the change of excess loss coefficient with magnetic flux density affects the total core loss as well as the ratio of rotating and alternating core losses. In addition, it is observed from Fig. 12 that the lines for hysteresis loss and eddy current loss plus hysteresis loss seem overlapping to each other which indicates that the effect of eddy current loss of the amorphous material is very small.

In the second method [20], the rotational excess loss can be obtained from the alternating excess loss data as the same as that of alternating loss based rotational hysteresis model in (6).

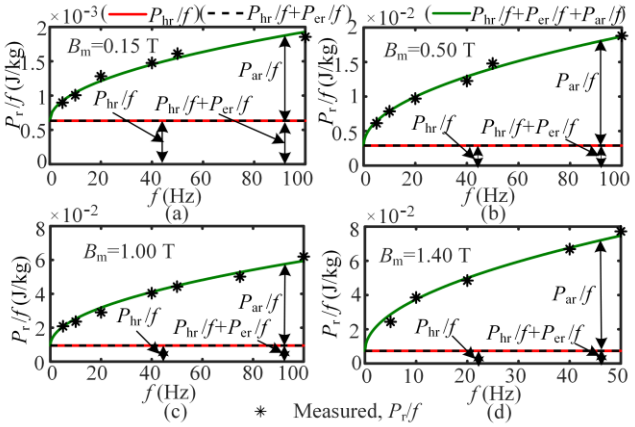


Fig. 12. Curve fitting of the measured core loss data with frequency for different maximum magnetic flux densities, e.g. (a) 0.15 T, (b) 0.50 T, (c) 1.00 T and (d) 1.40 T.

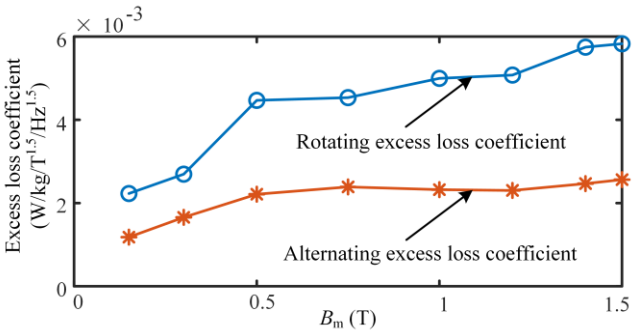


Fig. 13. Rotating and alternating excess loss coefficients with magnetic flux density.

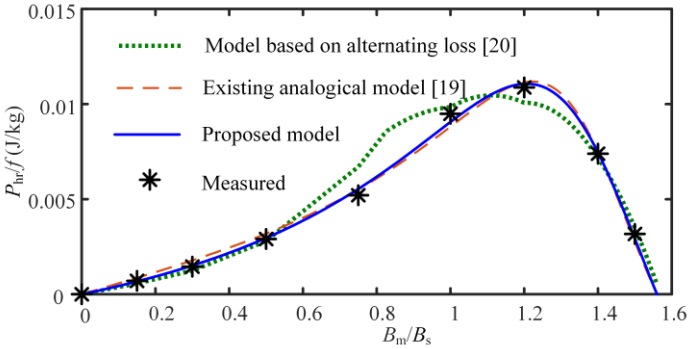


Fig. 14. Comparison of different models for modelling rotational hysteresis loss of the amorphous magnetic material.

## V. Modelling of Alternating Core Loss

The loss separation method is also used for modelling of the alternating core loss. The alternating eddy current and

excess losses are modelled in the same as the rotational core loss model. However, the pattern of the alternating hysteresis loss is quite different from the rotational hysteresis loss especially at the situation near to the $B_s$. As the total loss is the sum of hysteresis, eddy current and excess losses, the total alternating loss $P_{alt}$ can be expressed as

$$P_{alt} = P_{ha} + \frac{\sigma \pi^2 d^2}{6\rho} B_m^2 f^2 + C_{aa} B_m^{1.5} f^{1.5} \tag{13}$$

where $C_{aa}$ is the alternating excess loss coefficient. The calculations of the $P_{ha}$ and $C_{aa}$ are carried out as the same as that for the rotational core loss. The calculated alternating excess loss coefficient with magnetic flux density is shown in Fig. 13. From Fig. 13, it is seen that the rotating excess loss coefficient is higher than the alternating excess loss coefficient. In the low magnetic flux density region, e.g. up to 0.5 T, both coefficients increase but after that the alternating excess loss coefficient becomes almost constant. On the other hand, the rotating excess loss coefficient shows an increasing trend. However, the modellings of alternating eddy current and excess losses are already included in the last two terms of the right side of (13) respectively. The rest term which is the alternating hysteresis loss can be modelled by the following Steinmetz equation [24]:

$$P_{ha} = C_{ha} B_m^{\beta} f \tag{14}$$

where $C_{ha}$ and $\beta$ are the Steinmetz parameters which are obtained by curve fitting of hysteresis loss data.

## VI. Modeling of Elliptical Loss

The elliptical rotational core loss model was done by an analytical approach reported in [19]. In the analytical approach, some assumptions are considered such as the ratio of minor and major axes of loci of **B** is equal to that of loci of **H**, and the components of **H** on both axes are sinusoidal. The expression of elliptical loss is then written as [19]:

$$P_t = R_B P_r + \left(1 - R_B\right)^2 P_{alt} \tag{15}$$

where $R_B$ is the ratio of minor and major axes of the elliptical **B** loci.

## VII. Experimental verification

This section presents the experimental verification of the proposed rotational hysteresis loss model, and compares it with other models. Accordingly, the modellings of the rotational loss, alternating loss and elliptical core losses are also carried out and experimentally verified.

The proposed rotational hysteresis model is verified by curve-fitting the rotational hysteresis losses with respect to the $B_m$. To assess the accuracy of the model, the error is defined as follows [19]:

$$Error = \frac{\sqrt{\frac{1}{N-1}\sum_{i=1}^{N}\left(P_{i(test)} - P_{i(cal)}\right)^2}}{\max\left(P_{i(test)}\right)} \tag{16}$$

where $N$ is number of measured data, $P_{i(test)}$ the measured data and $P_{i(cal)}$ the calculated data. The optimization technique with considering the minimum error is applied for calculating the parameters of analogical rotational hysteresis models. The above-mentioned hysteresis models are applied to model the amorphous magnetic material. Fig. 14 (Section IV.C) shows the comparison among their results with the measured values. It is observed from Fig. 14 that the proposed model achieves a better agreement with the measured values than other models. The error for the proposed model is 2.11% whereas it is 3.55% and 6.42% for the existing analogical model and alternating loss-based model respectively.

Fig. 9 (Section III.B) shows the comparison among the simulation results and experimental results of the rotational core losses. It is observed from Fig. 9 that the analogical approach achieves a better agreement with the experimental results than the alternating loss-based approach.

Fig. 8 (Section III.B) shows the simulated and measured alternating losses. It is observed from Fig. 8 that the simulated results are close to the measured results. For the elliptical core loss, the simulation results also agree with the experimental results, although there exist small errors in the middle range of the axis ratio as shown in Fig. 11 (Section III.C). As the analytical model, which is used for the simulation, is based on some approximations discussed in Section VI, it shows small errors with the experimental results especially in the middle of the axis ratio range. In addition, in both rotational and alternating excess loss models, the excess loss is considered to be proportional to $(B_m f)^{3/2}$ as shown in (11) and (13), which is not a generalized approach for all types of magnetic materials as a perfect alignment of magnetic domains of the magnetic materials with magnetic field is hardly possible. Therefore, the aforementioned excess loss model introduces a small error in the calculation of core loss. Moreover, in this research the effect of temperature change and mechanical stress have not been considered in the measurement and modelling processes.

## VIII. Conclusion

Two-dimensional magnetic properties of the selected Fe-based amorphous magnetic material are measured and investigated under different excitation conditions. From the investigation, some remarkable results have been obtained, which are: (i) the rotational hysteresis loss of the amorphous magnetic material decreases at the vicinity of the saturated magnetic flux density which is similar to that of the silicon steels; (ii) the permeability differs slightly with the change of the direction of the magnetic field; (iii) the ratio of the rotational to alternating core losses is about 1.90, and decreases dramatically at the vicinity of saturation magnetic flux density; and (iv) for elliptical rotational core loss, the small change of axis ratio near to the peak axis ratio highly affects the total core loss. In addition, a simple improved

rotational hysteresis loss model is proposed and experimentally verified. It is also observed that the proposed model achieves a better agreement with measured data compared to others. Moreover, alternating and elliptical rotating core losses are modelled and compared with the measured results. The proposed model and the measured magnetic properties of the amorphous magnetic material can be used to design high-performance electromagnetic devices, e.g. electrical motors.

## REFERENCES


[1] J. C. Akiror, J. Wanjiku, P. Pillay, J. Cave, and A. Merkhouf, "Rotational core loss magnetizer: design and measurements," *IEEE Trans. Ind. Appl.*, vol. 54, no. 5, 4355–4364, Sep.-Oct. 2018.

[2] J. G. Zhu, "Numerical modelling of magnetic materials for computer aided design of electromagnetic devices," *Ph.D. Dissertation*, School of Electrical Engineering, University of Technology Sydney, Australia, Jul. 1994.

[3] N. Ertugrul, R. Hasegawa, W. L. Soong, J. Gayler, S. Kloeden, and S. Kahourzade, "A novel tapered rotating electrical machine topology utilizing cut amorphous magnetic material," *IEEE Trans. Magn.*, vol. 51, no. 7, Jul. 2015, Art. 8106006.

[4] Z. Wang, *et al*., "Development of a permanent magnet motor utilizing amorphous wound cores," *IEEE Trans. Magn.*, vol. 46, no. 2, pp. 570–573, Feb. 2010.

[5] S. Kahourzade, N. Ertugrul, and W. L. Soong, "Loss analysis and efficiency improvement of an axial-flux PM amorphous magnetic material machine," *IEEE Trans. Ind. Electron*., vol. 65, no. 7, pp. 5376–5383, Jul. 2018.

[6] Henan ZY Amorphous Technology Co. Ltd. [Online]. Available: https://www.zyamorphous.com/. Accessed on. 22 Jul. 2020.

[7] Guangzhou Amorphous Electronic Technology Co. Ltd. [Online]. Available: https://coilcore.en.alibaba.com/. Accessed on. 22 Dec. 2020.

[8] S. Sahoo, "Review on vertical twin-roll strip casting: a key technology for quality strips," *J. Metall.*, vol. 2016, Aug. 2016; Art. 1038950.

[9] A. Krings, A. Boglietti, A. Cavagnino, and S. Sprague, "Soft magnetic material status and trends in electric machines," *IEEE Trans. Ind. Electron.*, vol. 64, no. 3, pp. 2405–2414, Mar. 2017.

[10] F. G. Baily, "The hysteresis of iron and steel in a rotating magnetic field," *Phil. Trans. Royal Soc. A*, vol. 187, pp. 715–746, Sep. 1896.

[11] W. Brix, K. Hempel, and F. Schulte, "Improved method for the investigation of the rotational magnetization process in electrical steel sheets," *IEEE Trans. Magn.,* vol. 20, no. 5, pp. 1708–1710, Sep. 1984.

[12] P. J. Flanders, "The rotating-sample magnetometer," *J. Appl. Phys.*, vol. 38, no. 3, pp. 1293–1294, Mar. 1967.

[13] J. Sievert, H. Ahlers, M. Enokizono, S. Kauke, L. Rahf, and J. Xu, "The measurement of rotational power loss in electrical sheet steel using a vertical yoke system," *J. Mag. Magn. Mat.*, vol. 112, no. 1–3, pp. 91–94, Jul. 1992.

[14] Y. G. Guo, J. G. Zhu, and J. J. Zhong, "Measurement and modelling of magnetic properties of soft magnetic composite material under 2D vector magnetisations," *J. Mag. Magn. Mat.,* 302, no. 1, pp. 14–19, Jul. 2006.

[15] M. Enokizono, T. Suzuki and J. D. Sievert, "Measurement of iron loss using rotational magnetic loss measurement apparatus," *IEEE Trans. J. Magn. Jpn.*, vol. 6, no. 6, pp. 508–514, Jun. 1991.

[16] A. Cecchetti, G. Ferrari, F. Masoli, and G. Soardo, "Rotational power losses in 3% SiFe as a function of frequency," *IEEE Trans. Magn*., vol. 14, no. 5, pp. 356–358, Sep. 1978.

[17] S. Ueno, T. Todaka, and M. Enokizono, "Measurement of vector magnetic properties of Fe–Si–B amorphous material," *IEEE Trans. Magn*., vol. 47, no. 10, pp. 3188–3191, Oct. 2011.

[18] M. Enokizono, G. Shirakawa, and J. Sievert, "Anomalous anisotropy and rotational magnetic properties of amorphous sheet," *J. Magn. Magn. Mater*., vol. 112, no. 1–3, pp. 195–199, Jul. 1992.

[19] J. G. Zhu and V. S. Ramsden, "Improved formulations for rotational core losses in rotating electrical machines," *IEEE Trans. Magn*., vol. 34, no. 4, pp. 2234–2242, July 1998.

[20] Y. Gao, *et al*., "Simple numerical calculation method of rotational iron loss in silicon steel sheets," *IEEE Trans. Magn.*, vol. 55, no. 6, Jun. 2019, Art. 6300404.

[21] J. G. Zhu and V. S. Ramsden, "Two dimensional measurement of magnetic field and core loss using a square specimen tester," *IEEE Trans. Magn.*, vol. 29, no. 6, pp. 2995–2997, Nov. 1993.

[22] T. Yamaguchi and K. Narita, "Rotational power loss in commercial silicon-iron laminations," *Elect. Eng. Jpn.*, vol. 96, no. 4, pp. 15–21, Jul. 1976.

[23] S. J. Chapman, "Electric Machinery Fundamentals," *McGraw Hill*, New York, 5th Edition, Feb. 2011.

[24] C. P. Steinmetz, "On the law of hysteresis," *Proc. IEEE*, vol. 72, no. 2, pp. 197–221, Feb. 1984.